Thin Coatings of α- and β-Bi₂O₃ by Ultrasonic Spray Coating of a Molecular Bismuth Oxido Cluster and their Application for Photocatalytic Water Purification Under Visible Light

Max Hofmann,[a, b] Leonard Rößner,[c] Marc Armbrüster,[c] and Michael Mehring*[a, b]

Thin coatings of Bi_2O_3 were deposited on glass substrates by ultrasonic spray coating of THF solutions of the molecular precursor $[Bi_{38}O_{45}(OMc)_{24}(DMSO)_9] \cdot 2DMSO \cdot 7H_2O$ (OMc = $O_2CC_3H_5$) followed by hydrolysis and subsequent annealing. Depending on the synthetic protocol, the bismuth oxido cluster was transformed into either α- or β-Bi_2O_3. The as-synthesized Bi_2O_3 coatings were characterized by powder X-ray diffraction (PXRD), thickness measurements, diffuse reflectance UV-Vis spectroscopy (DRS), photoluminescence (PL) spectroscopy, Raman spectroscopy and scanning electron microscopy (SEM). The thin coatings (thickness: 5–16 μm) were compared with regard to their performance in photocatalytic rhodamine B (RhB) decomposition under visible light irradiation. The β-Bi_2O_3 coatings, that showed the highest photocatalytic activity, were used for the photocatalytic decomposition of other pollutants such as triclosan and ethinyl estradiol. In addition, the interplay between the photooxidation that is induced by the excitation of the catalyst using visible light and the photosensitized decomposition pathway was studied by degradation experiments of aqueous rhodamine B solutions using β-Bi_2O_3 coatings.

1. Introduction

The preparation, modification and photocatalytic evaluation of semiconductors are an ongoing focus of research since the report of the UV light-driven photocatalytic activity of TiO_2 in the early 1970s.[1] Several bismuth-based chalcogenides (e.g. Bi_2O_3,[2,3] Bi_2S_3,[4] BiOCl)[5] and heterometallic oxides (e.g. $BiWO_6$,[6] $BiVO_4$,[7–10] $Ba(BiO_3)_2$,[11] $NaBiO_3$)[12] are suitable as advanced photoredox catalysts targeting visible-light response.[13] Bismuth oxide, which is classified as a non-toxic compound with a high LD_{50} value of 5000 mg/kg (rat, oral),[14] is an emerging candidate for the photocatalytic degradation of organic compounds in wastewater such as dye pollutants, biocides or drug residues. The decomposition of the biocide triclosan and the medicinal drug ethinyl estradiol in wastewater is an important research target. Although their concentrations are still below the legal limit, their inlet as well as their outlet concentrations to sewage treatment plants are already above the detection limits of the routinely used analytical instruments, which was exemplarily monitored for two German cities.[15] Residuals like the antimicrobial agent triclosan can be a problem for the so-called secondary treatment, that is based on the use of microorganisms in sewage plants. Ethinyl estradiol is known for its high estrogenic activity even at concentrations already present in the environment, which can disrupt amphibian mating behavior for example. Therefore, residuals of ethinyl estradiol might contribute to the worldwide problem of amphibian decline.[16] Previous investigations on dispersions of tetragonal β-Bi_2O_3 nanoparticles have proven their excellent efficiencies by decomposing the initial amount of ethinyl estradiol and triclosan.[3]

In addition to the tetragonal β-Bi_2O_3, the monoclinic α-Bi_2O_3 and the cubic δ-Bi_2O_3 polymorphs exhibit favorable visible-light response.[17] However, β-Bi_2O_3 revealed the best photocatalytic performance under visible light irradiation in comparative studies on single-phase oxides with regard to the decomposition of organic molecules like methyl orange and 4-chlorophenol.[18] Recently, we have shown that nanoparticles of the metastable polymorph β-Bi_2O_3 are easily accessible by a controlled hydrolysis process under mild conditions of poly-nuclear bismuth oxido clusters due to their structural relationship between the well-defined precursor and the tetragonal phase β-Bi_2O_3.[2]

However, an implementation of photocatalysts based on bismuth oxide nanoparticles into sewage treatment plants or their use in decentral solutions for wastewater treatment is hampered by cost-intensive separation of the catalyst nano-

[a] M. Hofmann, Prof. Dr. M. Mehring
     Fakultät für Naturwissenschaften
     Institut für Chemie, Professur Koordinationschemie
     Technische Universität Chemnitz
     Straße der Nationen 62, 09107 Chemnitz (Germany)
     E-mail: michael.mehring@chemie.tu-chemnitz.de
[b] M. Hofmann, Prof. Dr. M. Mehring
     Center for Materials, Architectures and Integration of Nanomembranes (MAIN)
     Rosenbergstraße 6, 09126 Chemnitz (Germany)
[c] L. Rößner, Prof. Dr. M. Armbrüster
     Fakultät für Naturwissenschaften
     Institut für Chemie, Professur Materialien für innovative Energiekonzepte
     Technische Universität Chemnitz
     Straße der Nationen 62, 09107 Chemnitz (Germany)

     Supporting information for this article is available on the WWW under https://doi.org/10.1002/open.201900323

particles from the purified water and their potential nano-toxicity, which is getting important in case of particle leaching.[19] Therefore, recent studies focused on immobilization concepts with main emphasis given to well-established photo-catalysts like titanium dioxide.[20–22] So far, a limited number of studies has been reported for the production of single-phase β-Bi_2O_3 coatings including low-pressure chemical vapor deposition (CVD) starting from bismuth(III) tert-butoxide. The resulting semiconductor films were shown to be suitable for UV-light induced oxygen evolution from water in the presence of a sacrificial agent.[23] In addition, a high visible-light-harvesting potential and incident photon-to-electron conversion efficiency were shown for β-Bi_2O_3 nanoporous films obtained by radio frequency magnetron sputtering using Bi targets[24] and sol-gel spin coating of a solution of bismuth(III) nitrate pentahydrate in the presence of additives such as an ethanolic solution of triton X-100 and citric acid.[25] The water purification efficiency of single-phase tetragonal β-Bi_2O_3 coatings synthesized by spray pyrolysis using bismuth(III) acetate as the precursor was evaluated for the degradation of organic dye solutions like methyl orange, acid blue 113, rhodamine B and indigo carmin under UV and visible light.[26,27] Photochemical solution deposition using the photosensitive bismuth(III)-N-meth-yldiethanolamine complex is another suitable preparation method in order to immobilize tetragonal β-Bi_2O_3. Efficient photodegradation of an aqueous methylene blue solution with a UV light source was demonstrated in the presence of the as-prepared films.[28,29] In addition, in situ growth of Bi_2O_3 on a Cu surface starting with bismuth(III) nitrate pentahydrate provides β-Bi_2O_3 films as well.[30] To prove the photoelectric conversion performance, the immobilized catalysts were placed into a cell under chopped visible light irradiation.

Herein, we report an alternative preparation method for immobilized Bi_2O_3 polymorphs, based on ultrasonic spray coating.[31] This cold spray technique enables an easy scale-up from the laboratory scale to dimensions much larger in size, which would be needed for wastewater treatment plants. In addition, ultrasonic spray coating is quite flexible with regard to the choice of material characteristics of the substrates. Although dispersions might be used in ultrasonic spray coating, the use of molecular precursors, which are soluble in organic solvents, is favorable as this produces more uniform films. The most common starting material bismuth(III) nitrate pentahydrate is not suitable because it is only soluble with appropriate amounts under highly acidic aqueous conditions. Therefore, the previously reported bismuth oxido cluster $[Bi_{38}O_{45}(OMc)_{24}(DMSO)_9]\cdot 2DMSO\cdot 7H_2O$, which is easily accessible and soluble in a broad range of solvents due to its organic ligand shell working as solubility enhancer, was used in this study.[32] We present the ultrasonic spray coating of this cluster followed by a hydrolysis and annealing protocol. Thus, thin coatings of α- and β-Bi_2O_3 were prepared and their photo-catalytic activity for the degradation of organic molecules such as rhodamine B under visible light irradiation was studied. Even more relevant to wastewater treatment, degradation experiments on the biocide triclosan and the medicinal drug ethinyl estradiol were performed using the as-prepared photocatalytic coatings.

2. Results and Discussion

2.1. Thin Coating Formation

Thin coating formation of photoactive semiconductors was realized using a cold spray technique. The general concept of the preparation of Bi_2O_3 thin films by this ultrasonic spray coating starting with the well-defined bismuth oxido cluster $[Bi_{38}O_{45}(OMc)_{24}(DMSO)_9]\cdot 2DMSO\cdot 7H_2O$ is summarized in Scheme 1. First, the molecular precursor $[Bi_{38}O_{45}(OMc)_{24}(DMSO)_9]\cdot 2DMSO\cdot 7H_2O$ was dissolved in THF to give a colorless solution that was spray coated on a glass substrate. Constant heating of the substrate to 80 °C through-out the spray process ensured the removal of the solvent and film formation of the cluster on the substrate. The as-deposited bismuth oxido cluster was then hydrolyzed by dipping the substrate into an aqueous sodium hydroxide solution for 60 min. The samples were annealed at 370 °C in a tube furnace for 15 min under argon flow resulting in single-phase β-Bi_2O_3 coatings (Figure 1a, β-Bi_2O_3-1). Coatings of the monoclinic phase (Figure 1a, α-Bi_2O_3-1) are obtained by an annealing protocol using higher temperatures (550 °C for 15 min). Comparison of the powder X-ray patterns of α-Bi_2O_3 films resulted in strong deviations of the observed and calculated intensities of the reflections. Further analysis revealed a preferred orientation of the crystallites and applying the model for oriented platelets
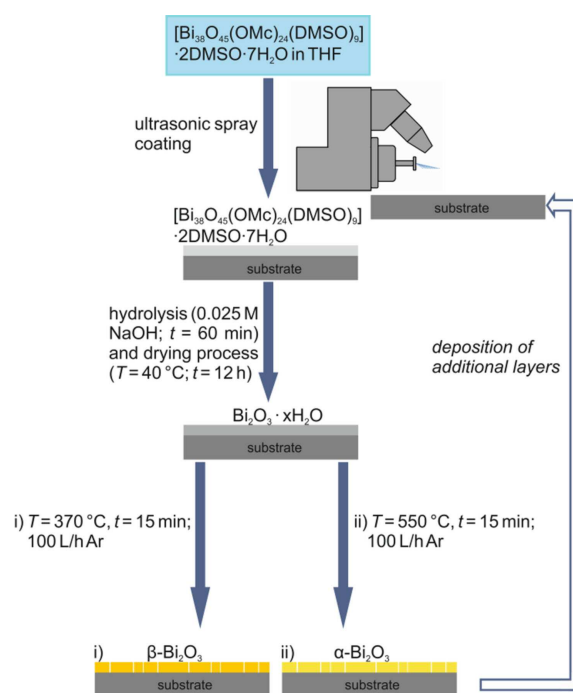
Scheme 1. General concept for the preparation of i) α-Bi_2O_3 and ii) β-Bi_2O_3 coatings by ultrasonic spray coating starting with a well-defined bismuth oxido cluster.
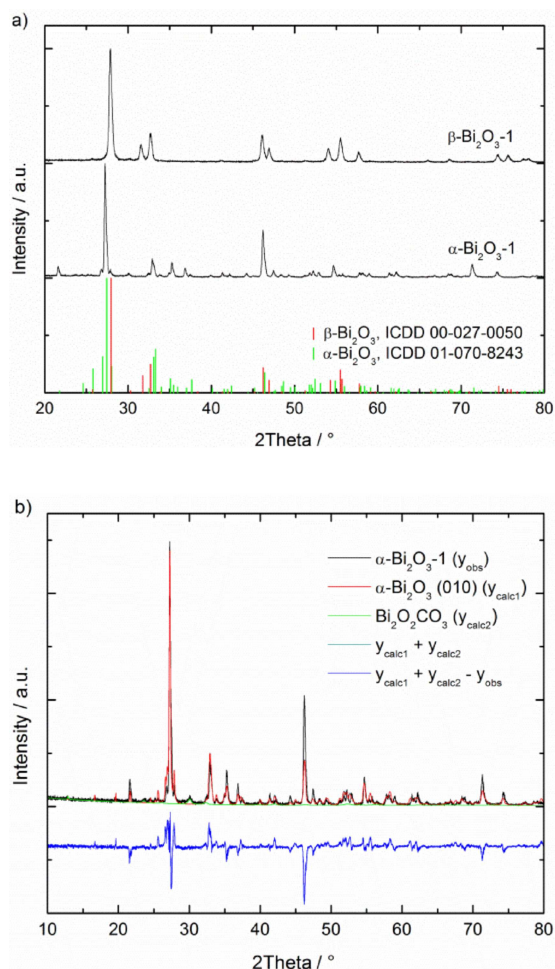
Figure 1. a) Powder XRD patterns of as prepared thin coatings of α-Bi$_2$O$_3$-1 and β-Bi$_2$O$_3$-1 (references: β-Bi$_2$O$_3$, ICDD 00-027-0050, red line; α-Bi$_2$O$_3$, ICDD 01-070-8243, green line).[35,36] b) i) Measured pattern of α-Bi$_2$O$_3$-1 (y$_{obs}$, black line), the calculated intensities of the reflections for ii) 94.7 wt% α-Bi$_2$O$_3$ with a preferred (010)-orientation (y$_{calc1}$, red line) and for iii) 5.3 wt% Bi$_2$O$_2$CO$_3$ (y$_{calc2}$, green line) as well as iv) the sum pattern (y$_{calc1}$ + y$_{calc1}$, blue line).

Figure 2. a) UV/Vis diffuse reflectance spectra of the as-prepared samples α-Bi$_2$O$_3$-1 and β-Bi$_2$O$_3$-1. b) Tauc plots (for direct band gap transition) calculated from the UV/Vis diffuse reflectance spectra of the pure polymorphs.

of *Toraya* and *Marumo* resulted in a (010)-oriented platelets with the values P1 = 0.98 and P2 = 0 after fitting the data with PowderCell (Figure 1b).[33,34]

The Bi$_2$O$_3$ coatings show absorption in the visible-light region (Figure 2a), whereby β-Bi$_2$O$_3$ shows the higher absorption edge at 552 nm. The band gaps determined based on Tauc plots using $(\alpha h\nu)^{2/n}$ ($n = 1$) versus $h\nu$ (Figure 2b) are (2.78 ± 0.03) eV for α-Bi$_2$O$_3$-1 and (2.34 ± 0.03) eV for β-Bi$_2$O$_3$-1. The visible light response of the monoclinic coating is in the range of values as reported for α-Bi$_2$O$_3$ in literature (2.8 eV).[37] The direct band gap value for the as-prepared β-Bi$_2$O$_3$ coating is lower than the value for β-Bi$_2$O$_3$ nanoparticles [(2.44 ± 0.03) eV], that were prepared starting from the analogous bismuth oxido cluster,[3] and slightly higher than reported for porous β-Bi$_2$O$_3$ (2.27 eV) by *Luo et al.*[38]

As exemplarily shown in Figure 3 for β-Bi$_2$O$_3$-1, the coatings have a block-like structure. The breaking-up of the layers is due to the removal of solvent residuals during the annealing process. The associated volume reduction led to tensions and
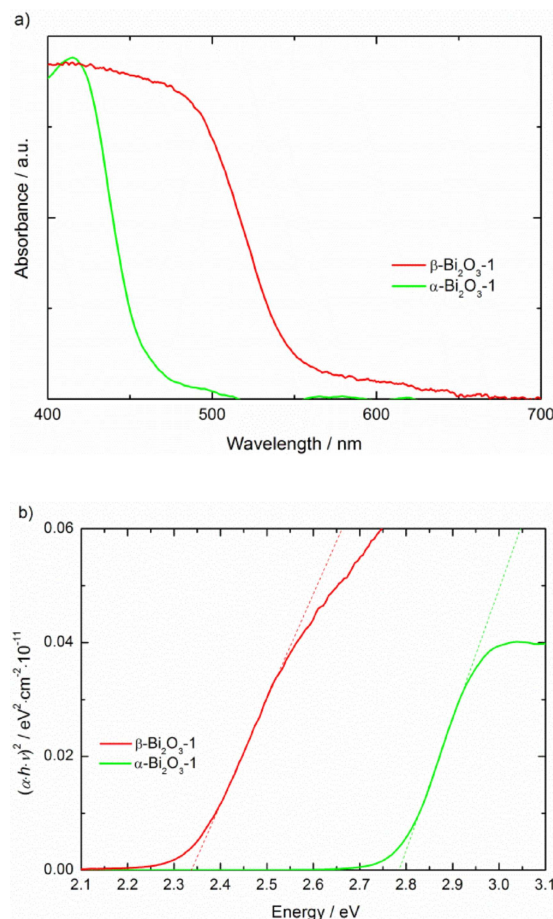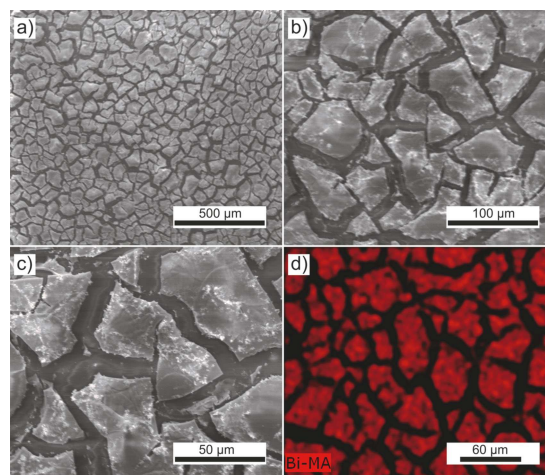

Figure 3. SEM images of the sample β-Bi$_2$O$_3$-1 magnified by factors of a) 100×, b) 500× and c) 1000×. Corresponding EDX mapping results are shown for d) Bi (magnification: 589×).

microcracking in the end, similar to nature, when soils dry out, and well known for TiO$_2$ films after thermal treatment.[39] This effect can also be observed for α-Bi$_2$O$_3$-1 (Figure S1). Therefore,

the glass substrates are not completely covered with Bi_2O_3 as evidenced by EDX mapping. However, microstructuring and its positive impact on the specific surface area can be beneficial for the catalytic properties. The thickness of the coating is (8 ± 4) µm according to the eddy current method using electrically conductive substrates like a silver sheet as well as a molybdenum sheet coated with β-Bi_2O_3. In comparison, analyzing SEM images (Figure S2) gives (5 ± 1) µm coating thickness on a glass substrate. Exemplarily, the scotch tape adhesion test was performed on sample β-Bi_2O_3-1 to get a qualitative idea of the adhesion of the Bi_2O_3 coatings on the substrates. The as prepared coatings are not fully resistant to external forces, since the scotch tape came off with some Bi_2O_3 stuck to it (Figure S3). Nevertheless, the coatings remain adhered to the substrate in stirred solutions without mass loss during photocatalytic testing as shown by differential weighing. In addition, AAS measurements of the remaining test solutions yielded a negligibly small mass of (1.9 ± 0.3) µg Bi in total (Bi_2O_3 in solution after 10.5 h of catalysis: 0.004% coating mass from β-Bi_2O_3-3).

2.2. Photocatalytic Testing and Optimization of the Bi_2O_3 Coatings

For comparison, the photocatalytic activity of the different polymorphs of the Bi_2O_3 coatings was evaluated in a reactor using 35 mL rhodamine B solution $(1\times10^{-5}$ M) under visible light irradiation (Figure S4). Before illumination, the time for establishing the adsorption-desorption equilibrium was determined experimentally for the test solution (Figure S5). In addition, a photolysis experiment with a blank glass substrate was performed. The sample α-Bi_2O_3-1 shows only a low photodegradation performance. After 600 min, the RhB conversion was 24% for α-Bi_2O_3-1, which is only a slight improvement over photolysis (17%). The thin coating of β-Bi_2O_3 (β-Bi_2O_3-1) was more active with a conversion of 33% after 600 min, which corresponds to a reaction rate constant of $0.60\cdot10^{-3}$ min^{-1} (Figure S6, Table S1). The higher activity of β-Bi_2O_3 as photocatalyst in comparison to α-Bi_2O_3 (Table S1) is in accordance with previous studies investigating decomposition of several pollutants under visible light irradiation using Bi_2O_3 dispersions.[18,40–44]

For the Bi_2O_3 coatings we observed an incomplete coverage of the substrate, which was believed to limit the photocatalytic activity. Therefore, yet another preparation pass was performed using a β-Bi_2O_3-1 sample as starting substrate. The deposited $[Bi_{38}O_{45}(OMc)_{24}(DMSO)_9]\cdot2DMSO\cdot7H_2O$ layers on top of the Bi_2O_3 coating were treated in analogy to the preparation method used before. The annealing process was performed at 370 °C under argon atmosphere to give single-phase β-Bi_2O_3 (β-Bi_2O_3-2, Figure 4). Moreover, the as-obtained β-Bi_2O_3-2 samples were also used as starting material for a third preparation cycle. The powder XRD patterns of thus prepared β-Bi_2O_3-3 show the tetragonal phase, whereby the small shoulder at $2\Theta=27.3°$ (*) might be indicative of the monoclinic phase as minor impurity (Figure 4). Thus it is demonstrated that a step by step deposition of β-Bi_2O_3 layers is possible. The mass of Bi_2O_3 per
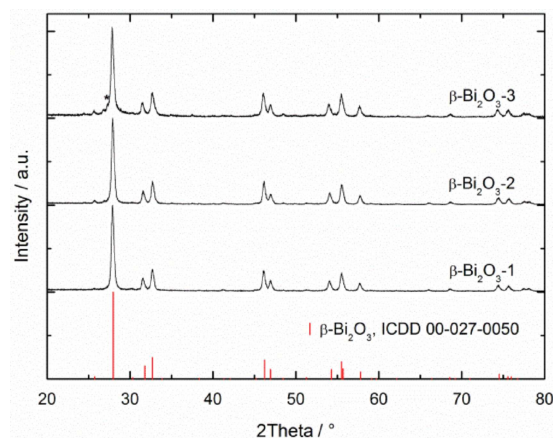
Figure 4. Powder XRD patterns of the as-obtained coatings after performing the preparation cycle once (β-Bi_2O_3-1), twice (β-Bi_2O_3-2) and thrice (β-Bi_2O_3-3) (references: β-Bi_2O_3, ICDD 00-027-0050, red line).[35]

unit area on the substrate was determined to be 2.8 mg·cm^{-2} (β-Bi_2O_3-1), 5.6 mg·cm^{-2} (β-Bi_2O_3-2) and 8.4 mg·cm^{-2} (β-Bi_2O_3-3). Simultaneously with the mass of the coatings the thickness increased (β-Bi_2O_3-1: (5 ± 1) µm, β-Bi_2O_3-2: (11 ± 6) µm, β-Bi_2O_3-3: (16 ± 4) µm) due to the additional deposits, which was monitored by SEM (Figure S2). EDX analysis revealed that the films are composed of bismuth and oxygen only and no residuals of sodium from the hydrolysis step were detected (Figure S7).

The morphology of the superimposed coatings (Figure 5) is similar to the observed block-like structure of β-Bi_2O_3-1 (Figure 3). Nevertheless, the positions of the stacked blocks are shifted resulting in a complete coverage of the substrates with Bi_2O_3. An optical distinction between the two-stacked coatings (β-Bi_2O_3-2) and the three-stacked coatings (β-Bi_2O_3-3) does not become obvious. The small channels at the surface are probably a result of the evaporation of residual solvent during the annealing process. UV/Vis diffuse reflectance spectra of the as-obtained samples do not differ significantly from β-Bi_2O_3-1
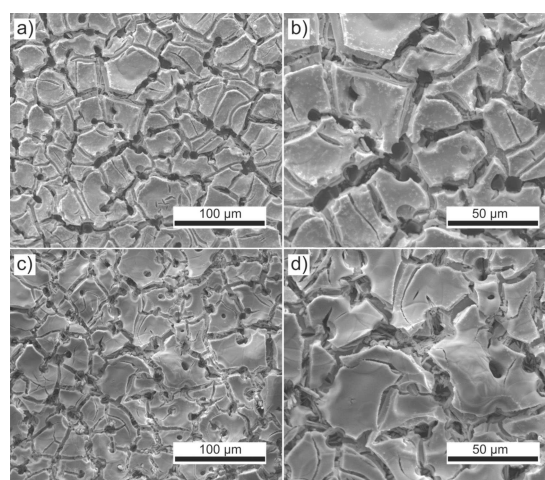
Figure 5. SEM images of two-stacked coating β-Bi_2O_3-2 [magnification: a) 500×, b) 1000×] and three-stacked coating β-Bi_2O_3-3 [magnification: a) 500×, b) 1000×].

(Figure S8a). Calculation of the optical band gaps based on Tauc plots give (2.32 ± 0.02) eV for both β-Bi$_2$O$_3$-2 and β-Bi$_2$O$_3$-3 (Figure S8b). With regard to the separation efficiency of photo-generated charges, no significant PL of the coatings is detected (Figure S9), which might be attributed to a low recombination rate of photo-induced electrons and holes.[45,46]

The photocatalytic efficiency of the as-prepared samples β-Bi$_2$O$_3$-2 and β-Bi$_2$O$_3$-3 was evaluated by experiments on the degradation of rhodamine B under visible light irradiation. The visible light spectra of the decolorization of a dye solution is exemplarily given for β-Bi$_2$O$_3$-3 (Figure 6). Notably, a slight hypsochromic shift becomes obvious, which might be indicative of a stepwise decomposition of *N,N,N',N'*-tetraethylrhodamine (rhodamine B) to give de-ethylated rhodamine intermediates.[47] This process is described as a photosensitized mechanism, whereby excited electrons of the organic molecule are transferred to the conduction band of the semiconductor. It was already shown for β-Bi$_2$O$_3$ nanoparticles that the photodegradation is a result of the interplay of the photosensitized degradation pathway in combination with the direct oxidation of the chromophoric system by photogenerated active
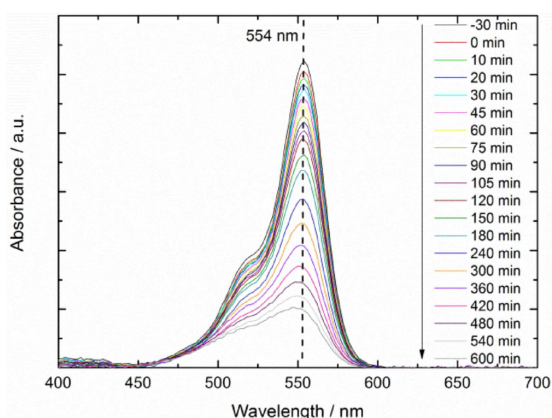
species.[3,48,49] The experiment in aqueous solution was repeated using a cut-off filter at 550 nm (OG550) to clarify the influence of the photosensitized mechanism. This cut-off filter nearly completely prevents the direct excitation of the semiconductor, but an excitation of rhodamine B is still possible ($\lambda = 554$ nm). The photocatalytic performance of β-Bi$_2$O$_3$-3 is significantly lower (24% rhodamine B conversion after 600 min) in comparison to the experiment using a cut-off filter at 420 nm (Figure S10). Nevertheless, the degradation efficiency of the photocatalyst is still higher as compared to the photolysis of rhodamine B. Thus, it is concluded that the photosensitized degradation pathway does apply here indeed but exhibits only a minor contribution to the decolorization of rhodamine B using the as-prepared β-Bi$_2$O$_3$ coatings.

Upon additional coating of the film β-Bi$_2$O$_3$-1, which was prepared by a single preparation pass, the photocatalytic efficiency was significantly increased (Figure 7, Figure S11), however the photocatalytic efficiencies of the films β-Bi$_2$O$_3$-2 and β-Bi$_2$O$_3$-3 are similar. Using a cut-off filter at 420 nm, the rhodamine B conversion after 600 min was approximately 75% for β-Bi$_2$O$_3$-2 as well as for β-Bi$_2$O$_3$-3, which is a significant improvement as compared to β-Bi$_2$O$_3$-1 (33%). The enhanced decolorization determined by UV/Vis spectroscopy is in good accordance with the lowered non-purgeable organic carbon (NPOC). Starting from 3.36 mg·mL^{-1} ($t = -30$ min) a value of 2.42 mg·mL^{-1} was achieved in the presence of β-Bi$_2$O$_3$-1 after 10 h of illumination, which was further lowered with the photocatalyst β-Bi$_2$O$_3$-3 (NPOC = 1.54 mg·mL^{-1}) proving a efficient oxidation of the dye to CO$_2$. It is concluded that a complete coverage of the substrate, which is associated with an higher amount of active centers at the surface, seems to be the key factor in order to maximize the photocatalytic efficiency of the Bi$_2$O$_3$ coatings, whereas the thickness of the coating seems to be negligible. The as-prepared sample β-Bi$_2$O$_3$-2 is favorable with regard to the amount of decolorized dye per irradiation time and per catalyst mass employed (Figure S12, Table S1). The catalytic activity of Bi$_2$O$_3$ itself in the sample β-Bi$_2$O$_3$-3 is reduced to 63% in comparison to the semiconductor material in the sample β-Bi$_2$O$_3$-2 due to the higher mass percentage embedded in the bulk material of the coating.

The XRD pattern of the sample β-Bi$_2$O$_3$-3 shows the formation of a minor amount of Bi$_2$O$_2$CO$_3$ in addition to β-Bi$_2$O$_3$ after 10 h of visible light irradiation in a RhB solution (Figure 8), which is confirmed by Raman spectroscopy (Figure S13). The reaction of β-Bi$_2$O$_3$ with CO$_2$, either formed *in situ* upon release during the photodegradation of organic compounds or as a result of contact with CO$_{2(aq)}$ under light irradiation, was discussed in previous studies on β-Bi$_2$O$_3$ particles.[3,50–53] In contrast, XRD studies of the samples α-Bi$_2$O$_3$-1 and β-Bi$_2$O$_3$-1 after the degradation experiments do not show any indication of photocorrosion (Figure S14, Figure S15), which is most likely the result of the lower photocatalytic activity (Table S1). Noteworthy, Bi$_2$O$_2$CO$_3$ itself is an efficient photocatalyst,[54] which might explain the negligible loss of activity. However, the β-Bi$_2$O$_3$/Bi$_2$O$_2$CO$_3$ mixture can be easily regenerated by annealing at 370 °C for 1 h in a furnace under an argon atmosphere to give single-phase β-Bi$_2$O$_3$. The recycled sample shows nearly the

Figure 6. Visible light spectra monitoring the photodegradation of rhodamine B (1·10^{-5} M) using β-Bi$_2$O$_3$-3 as photocatalyst ($t = -30$ min: start of stirring in the dark, $t = 0$ min: start of irradiation with visible light).
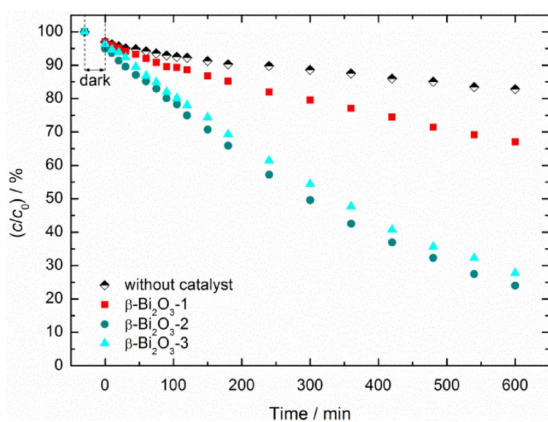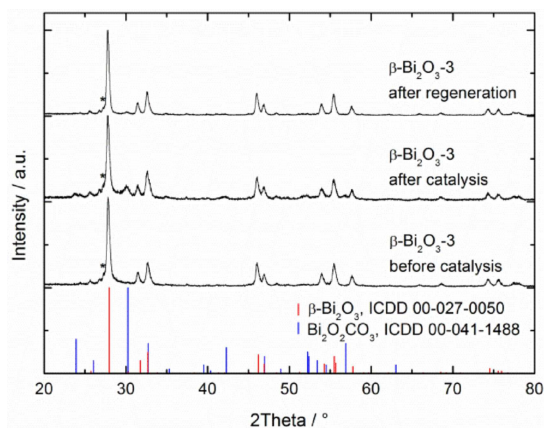

Figure 7. Time-dependent photodegradation of an aqueous rhodamine B solution (1·10^{-5} M) under visible light irradiation ($t > 0$ min) without catalyst and in the presence of β-Bi$_2$O$_3$-1, β-Bi$_2$O$_3$-2 and β-Bi$_2$O$_3$-3 as photocatalysts.

Figure 8. Powder XRD patterns of the sample β-Bi$_2$O$_3$-3 i) before photocatalysis, ii) after 10 h of rhodamine B degradation under visible light and iii) after regeneration at 370 °C for 1 h under an argon atmosphere (references: β-Bi$_2$O$_3$, ICDD 00-027-0050, red line; Bi$_2$O$_2$CO$_3$, ICDD 00-041-1488, blue line).[35,55]

same photodegradation efficiency as the pristine sample (Figure S16).

2.3. Photocatalytic Degradation of Further Pollutants

To probe the coatings for the degradation of other pollutants than rhodamine B, β-Bi$_2$O$_3$-3 samples were illuminated with visible light in 35 mL of $4 \cdot 10^{-5}$ M aqueous solutions of ethinyl estradiol and triclosan (Figure 9). The adsorption-desorption equilibriums are reached throughout a dark phase of 30 min (Figure S17, Figure S18). In the presence of β-Bi$_2$O$_3$-3 as immobilized photocatalyst, the initial concentrations are reduced to 53% for ethinyl estradiol and 17% for triclosan (Figure S19, Figure S20). In case of triclosan over 80% of the initial pollutant is removed from solution in the presence of β-Bi$_2$O$_3$-3 including adsorption on surfaces and photolysis, whereas 15% are decomposed solely during the irradiation time without using a catalyst. It can be summarized, that the
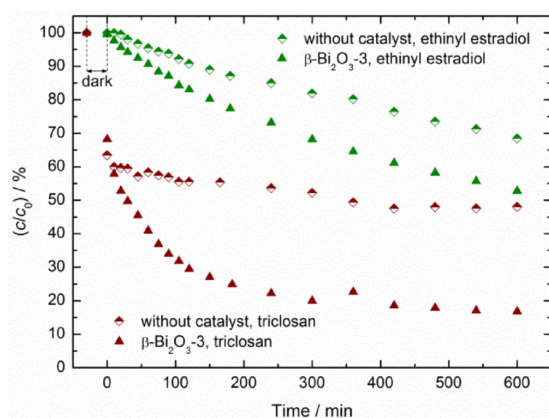
photocatalytic conversion of triclosan after 600 min exceeds its photolysis more than three times. Therefore, the immobilized photocatalysts can be a beneficial contribution for supplementary cleaning stages decreasing the concentration of the antimicrobial pollutant in wastewater. This can protect the so called secondary treatment, which makes use of aquatic microorganisms, from damage. However, the NPOC value ($5.77 \ mg \cdot mL^{-1}$) was not decreased, which shows that the biocide is not fully oxidized to CO$_2$. In case of ethinyl estradiol the NPOC was reduced from $9.61 \ mg \cdot mL^{-1}$ to $5.00 \ mg \cdot mL^{-1}$, which indicates partial removal of photooxidation products in the form of CO$_2$ from water samples.

3. Conclusions

Thin coatings of α-Bi$_2$O$_3$ and β-Bi$_2$O$_3$ are accessible starting from the well-defined bismuth oxido cluster [Bi$_{38}$O$_{45}$(OMc)$_{24}$(DMSO)$_9$]·2DMSO·7H$_2$O under mild conditions using ultrasonic spray coating. A modified hydrolysis and annealing protocol adapted from a nanoparticle synthesis was successfully transferred to the preparation route for immobilized Bi$_2$O$_3$ on different substrates composed of float glass, silver or molybdenum. Therefore, an implementation of the concept for various other substrate materials seems straightforward. As might be expected a significantly higher photocatalytic activity is observed for coatings composed of tetragonal Bi$_2$O$_3$ (β-Bi$_2$O$_3$-1) as compared to coatings composed of monoclinic Bi$_2$O$_3$ (α-Bi$_2$O$_3$-1). As-prepared samples by a repeated pass of the coating process (β-Bi$_2$O$_3$-2, β-Bi$_2$O$_3$-3) show significantly enhanced activity, whereby the crucial factor is a full coverage of the substrate for generating an higher amount of active sites rather than coating thickness. Thus a degradation efficiency of 74% of rhodamine B decomposition after 600 min of visible light irradiation was obtained. As expected the value is lower than observed for nanoparticle dispersions used as photocatalyst, but from a technological point of view the approach is promising for applications in sewage treatment plants. Even more important than studies on model compounds are photodegradation experiments using wastewater pollutants like the antimicrobial agent triclosan or ethinyl estradiol with its estrogenic activity. We have demonstrated partial removal of photooxidized ethinyl estradiol as well as rhodamine B in the form of CO$_2$. The as-prepared coatings β-Bi$_2$O$_3$-3 are able to decompose nearly half of the initial concentration of ethinyl estradiol and more than 80% in case of triclosan under visible light irradiation, which offers potential for further implementation in treatment stages.

Figure 9. Time-dependent photodegradation of aqueous ethinyl estradiol and triclosan solutions ($4 \cdot 10^{-5}$ M) under visible-light irradiation ($t > 0$ min) without catalyst and in the presence of β-Bi$_2$O$_3$-3 as photocatalyst.

Experimental Section

Chemicals

Bismuth(III) nitrate pentahydrate (Co. AlfaAesar) and sodium methacrylate (Co. AlfaAesar) were used as received. [Bi$_{38}$O$_{45}$(OMc)$_{24}$(DMSO)$_9$]·2DMSO·7H$_2$O was prepared according to a literature procedure.[32]

Spray Coating

Ultrasonic spray coating[56] as a cold spray technique[57] was carried out with a spray coating setup ExactaCoat Inert (Co. Sono-Tek) under argon atmosphere. The ultrasonic nozzle can move over a maximum area of 40×40 cm² and was adjusted within a sample-to-nozzle distance of 36 mm. The substrate is heated (maximum: 250 °C) during the deposition process (heating plate: 20×20 cm²). A piezoelectric quartz crystal is used to control the nozzle, and vibration with a fixed ultrasonic frequency (120 kHz) is provided. The solution passes (maximum: 19 mL min⁻¹) through an opening diameter of 1 mm and forms a thin liquid film on the nozzle tip. The amplitude of the wave generated by the vibration depends on the electrical power of 1.6 W being adjusted at the piezocrystal. The nozzle head translates with a velocity of 25 mm·s⁻¹ in 3 mm displaced traces.

Materials Characterization

Powder X-ray diffraction (XRD) was carried out with a STOE-STADI-P diffractometer equipped with a Ge(111)-monochromator. The X-ray source was CuK$_{\alpha 1}$-radiation (40 kV, 40 mA). Energy dispersive X-ray spectroscopy (EDX) and scanning electron microscopy (SEM) were performed using a NovaNano SEM (Co. FEI) with the following parameters: pressure ($\sim 10^{-5}$ mbar), work distance (4 to 6 mm) and acceleration voltage (5 to 30 kV) using a Si Drift Detector XFlash 3001 (Co. Bruker AXS). Diffuse reflectance UV-Vis spectroscopy was performed using a Carry 60 UV-Vis (Co. Agilent Technologies) equipped with a Barrelino™ (Co. Harrick Scientific Products) remote diffuse reflection probe. The band gap E_g of the semiconductor was estimated according to the equation $(\alpha h\nu) = A \cdot (h\nu - E_g)^{n/2}$, where α is the absorption coefficient of the material, $h\nu$ is the photon energy and A represents a proportionality constant. The parameter n indicates the nature of the fundamental optical transition. A direct transition is associated with a value of n = 1, whereas a semiconductor with an indirect transition is described with n = 4.[58] PL spectra of the samples were recorded using a Cary Eclipse (Fa. Varian) with an excitation wavelength of 380 nm. In addition, the fluorescence spectrophotometer was equipped with a 380 nm band-pass filter between radiation source and sample along with a 400 nm long-pass filter in front of the detector. The coating thickness measurement was carried out with a FISCHERSCOPE MMS PC2 (Co. Helmut Fischer GmbH) equipped with a plug-in module PERMASCOPE and a probe FTA3.3-5.6HF using an eddy current measuring method (DIN EN ISO 2360). The carbon content was determined using a FlashAE 1112 (Co. Thermo Scientific). The photocatalytic dye decomposition was analyzed by *in situ* UV-Vis spectroscopy using a Carry 60 UV-Vis (Co. Agilent Technologies) equipped with fiber optics. A Thermo Scientific iCE 3000 System was used for atomic absorption spectroscopy (AAS). The non-purgeable organic carbon (NPOC) was quantified in acidified solutions after purging the samples with oxygen by using a multi N/C 3100 TOC analyzer (Co. Analytik Jena). Raman spectra were recorded using a inVia Raman microscope (Co. Renishaw), and the laser excitation of a Nd:YAG (Nd:Y₃Al₅O₁₂) solid state laser ($\lambda = 532$ nm, $P_{max} = 50$ mW) was focused on the sample.

Preparation of β-Bi₂O₃ Coatings Starting from Ultrasonic Spray-Coated [Bi₃₈O₄₅(OMc)₂₄(DMSO)₉]·2DMSO·7H₂O

[Bi₃₈O₄₅(OMc)₂₄(DMSO)₉]·2DMSO·7H₂O is dissolved in tetrahydrofuran (25 g·L⁻¹). The colorless solution is used to produce thin films of the bismuth oxido cluster on float glass (23×25 mm, thickness: 1000 μm) by ultrasonic spray coating. The film is deposited repeating the spray process thirty times (30 spray cycles) with a flow rate of 0.5 mL·min⁻¹. The substrate is being completely scanned by the spray head above throughout each spray cycle and is preheated to 80 °C to enable the evaporation of the solvent. In a typical procedure, each bismuth oxido cluster coating is hydrolyzed with 0.025 M aqueous NaOH (50 mL) for 60 min and meanwhile the layer becomes turbid. After drying for 12 h at 40 °C, the sample is annealed in a furnace at 370 °C for 15 min (argon flow rate: 100 L·h⁻¹) and cooled down under argon atmosphere to give a yellow/orange coating with a mass of (16 ± 4) mg (2.8 mg·cm⁻²) deposited on the substrate (β-Bi₂O₃-1). The deposition of additional films is realized by repeating the spray coating process followed by hydrolysis and the annealing process. The samples β-Bi₂O₃-(1+x) (x = 0, 1) are used as substrates. Yellow/orange coatings with a mass of (32 ± 5) mg (5.6 mg·cm⁻²) for the sample β-Bi₂O₃-2 and (48 ± 2) mg (8.4 mg·cm⁻²) for the sample β-Bi₂O₃-3 are obtained after performing the preparation pass once more and twice more respectively. The residual carbon content is 0.12 % for β-Bi₂O₃-1.

Coatings on a silver sheet (23×25 mm, thickness: 250 μm, purity: 99.9 %) and a molybdenum sheet (23×25 mm, thickness: 100 μm, purity: 99.95 %) were prepared according to the as described procedure in order to perform the coating thickness measurements.

Preparation of α-Bi₂O₃ Coatings Starting from Ultrasonic Spray-Coated [Bi₃₈O₄₅(OMc)₂₄(DMSO)₉]·2DMSO·7H₂O

Starting from [Bi₃₈O₄₅(OMc)₂₄(DMSO)₉]·2DMSO·7H₂O the spray, hydrolysis and drying protocols are analogous to those for the β-Bi₂O₃ films. After drying, the sample is annealed in a furnace at 550 °C for 15 min (argon flow rate: 100 L h⁻¹) and cooled down under argon atmosphere to give a yellow coating with a mass of (16 ± 3) mg (2.8 mg·cm⁻²) deposited on the glass substrates (α-Bi₂O₃-1). The residual carbon content is 0.18 %.

Evaluation of Photocatalytic Activity

The photocatalytic activity of the as-prepared β-Bi₂O₃ coatings was evaluated in a water cooled glass reactor ($T = 15$ °C, Figure S21) using the coated carrier material and 35 mL of an aqueous solution of $1 \cdot 10^{-5}$ M rhodamine B (pH = 4.7), $4 \cdot 10^{-5}$ M triclosan (pH = 5.2), and $4 \cdot 10^{-5}$ M ethinyl estradiol (pH = 4.8). The reactor is equipped with a 300 W xenon lamp (type Cermax® VQTM ME300BF, Co. Perkin Elmer). A hot mirror filter ($\lambda \leq 700$ nm) is located within a distance of 12.3 cm at one side of the reactor and directly illuminates an area of 4.5 cm². A cut-off filter (λc (τi (τi = 0.50) = (420 ± 6) nm, GG420, Co. Schott) is used to remove the UV light. Before illumination, the solutions are stirred for 30 min in the dark to establish the adsorption-desorption equilibrium of the dye at the catalyst surface. The progress of photodegredation was studied by UV-Vis spectroscopy. The illumination process is interrupted by stopping the stirring and darkening the light beam by a cover prior to the UV-Vis measurement. The interval of measurement is timed every 10 min for the first 30 min, every 15 min between 30 to 120 min, every 30 min between 120 and 180 min and every 60 min to the last measurement after 600 min. The concentration of the pollutant is determined by calculating the area under the UV-Vis curve from 450–600 nm for RhB, 200–256 nm for triclosan and 235–315 nm for ethinyl estradiol. The photodegredation is plotted as a function of the irradiation time. Following the way of pseudo-first order reaction kinetics the logarithmic concentration of rhodamine B is plotted versus time to calculate the reaction rate constant k.

Keywords: thin coating · spray coating · bismuth oxide · photocatalysis · water purification

[1] A. Fujishima, K. Honda, *Nature* **1972**, *238*, 37–38.
[2] M. Schlesinger, S. Schulze, M. Hietschold, M. Mehring, *Dalton Trans.* **2013**, *42*, 1047–1056.
[3] M. Schlesinger, M. Weber, S. Schulze, M. Hietschold, M. Mehring, *ChemistryOpen* **2013**, *2*, 146–155.
[4] J. Arumugam, A. Dhayal Raj, A. Albert Irudayaraj, *J. Mater. Sci. Mater. Electron.* **2017**, *28*, 3487–3494.
[5] L. Ye, Y. Su, X. Jin, H. Xie, C. Zhang, *Environ. Sci.* **2014**, *1*, 90–112.
[6] S. Girish Kumar, K. S. R. Koteswara Rao, *Appl. Surf. Sci.* **2015**, *355*, 939–958.
[7] M. Hofmann, M. Rainer, S. Schulze, M. Hietschold, M. Mehring, *ChemCatChem* **2015**, *7*, 1357–1365.
[8] Z.-F. Huang, L. Pan, J.-J. Zou, X. Zhang, L. Wang, *Nanoscale* **2014**, *6*, 14044–14063.
[9] C. Martinez Suarez, S. Hernández, N. Russo, *Appl. Catal. A* **2015**, *504*, 158–170.
[10] K. Tolod, S. Hernández, N. Russo, *Catalysts* **2017**, *7*, 1–23.
[11] T. Takei, R. Haramoto, Q. Dong, N. Kumada, Y. Yonesaki, N. Kinomura, T. Mano, S. Nishimoto, Y. Kameshima, M. Miyake, *J. Solid State Chem.* **2011**, *184*, 2017–2022.
[12] C.-S. Lu, C.-C. Chen, L.-K. Huang, P.-A. Tsai, H.-F. Lai, *Catalysts* **2013**, *3*, 501–516.
[13] X. Meng, Z. Zhang, *J. Mol. Catal. A* **2016**, *423*, 533–549.
[14] S. R. Akhundov, *Gig. Tr. Prof. Zabol.* **1986**, *30*, 16–21.
[15] H. Fahlenkamp, C. B. Hannich, E. Möhle, T. Nöthe, T. Ries, *Chem. Ing. Tech.* **2004**, *76*, 1179–1189.
[16] F. Hoffmann, W. Kloas, *PLoS One* **2012**, *7*, 1–8.
[17] H. Zhao, F. Tian, R. Wang, R. Chen, *Rev. Adv. Sci. Eng.* **2014**, *3*, 3–27.
[18] H. Cheng, B. Huang, J. Lu, Z. Wang, B. Xu, X. Qin, X. Zhang, Y. Dai, *Phys. Chem. Chem. Phys.* **2010**, *12*, 15468–15475.
[19] M. Abudayyak, E. Öztaş, M. Arici, G. Özhan, *Chemosphere* **2017**, *169*, 117–123.
[20] A. Y. Shan, T. I. M. Ghazi, S. A. Rashid, *Appl. Catal. A* **2010**, *389*, 1–8.
[21] H. Zangeneh, A. A. L. Zinatizadeh, M. Habibi, M. Akia, M. Hasnain Isa, *J. Ind. Eng. Chem.* **2015**, *26*, 1–36.
[22] A. Ajmal, I. Majeed, R. N. Malik, H. Idriss, M. A. Nadeem, *RSC Adv.* **2014**, *4*, 37003–37026.
[23] S. J. A. Moniz, C. S. Blackman, C. J. Carmalt, G. Hyett, *J. Mater. Chem.* **2010**, *20*, 7881–7886.
[24] Y. Xin, L. Xiaojuan, L. Shangjun, W. Gang, J. Chunping, T. Jing, C. Jinwei, W. Ruilin, *J. Phys. D* **2013**, *46*, 1–6.
[25] X. Yang, X. Lian, S. Liu, C. Jiang, J. Tian, G. Wang, J. Chen, R. Wang, *Appl. Surf. Sci.* **2013**, *282*, 538–543.
[26] K. Barrera-Mota, M. Bizarro, M. Castellino, A. Tagliaferro, A. Hernandez, S. E. Rodil, *Photochem. Photobiol. Sci.* **2015**, *14*, 1110–1119.
[27] T. A. Gadhi, L. S. Gómez-Velázquez, M. Bizarro, A. Hernández-Gordillo, A. Tagliaferro, S. E. Rodil, *Thin Solid Films* **2017**, *638*, 119–126.
[28] D. Pérez-Mezcua, I. Bretos, R. Jiménez, J. Ricote, R. J. Jiménez-Rioboó, C. G. da Silva, D. Chateigner, L. Fuentes-Cobas, R. Sirera, M. L. Calzada, *Sci. Rep.* **2016**, *6*, 39561.
[29] D. Perez-Mezcua, I. Bretos, R. Jiménez, J. Ricote, R. J. Jiménez-Rioboó, C. G. da Silva, D. Chateigner, L. Fuentes-Cobas, R. Sirera, M. L. Calzada, *J. Sol-Gel Sci. Technol.* **2017**, *81*, 355–361.
[30] Y. Wang, Y. Long, D. Zhang, *J. Inst. Chem.* **2017**, *75*, 183–188.
[31] M. Hofmann, B. Büchter, M. Mehring, *Z. Anorg. Allg. Chem.* **2016**, *642*, 1047.
[32] L. Miersch, T. Rüffer, M. Mehring, *Chem. Commun.* **2011**, *47*, 6353–6355.
[33] H. Toraya, F. Marumo, *Mineral. J.* **1981**, *10*, 211–221.
[34] W. Kraus, G. Nolze, *PowderCell 2.4*, Federal Institute for Materials Research and Testing (BAM), Berlin **2013**.
[35] B. Aurivillius, G. Malmros, *Trans. Roy. Inst. Technol.* **1972**, *291*, 544–562.
[36] S. A. Ivanov, R. Tellgren, H. Rundlöf, V. G. Orlov, *Powder Diffr.* **2001**, *16*, 227–230.
[37] H.-Y. Jiang, G. Liu, P. Li, D. Hao, X. Meng, T. Wang, J. Lin, J. Ye, *RSC Adv.* **2014**, *4*, 55062–55066.
[38] X. Luo, G. Zhu, J. Peng, X. Wei, M. Hojamberdiev, L. Jin, P. Liu, *Appl. Surf. Sci.* **2015**, *351*, 260–269.
[39] M. Ulmann, N. R. De Tacconi, J. Augustynski, *J. Phys. Chem.* **1986**, *90*, 6523–6530.
[40] L. Shan, G. Wang, D. Li, X. San, L. Liu, L. Dong, Z. Wu, *Dalton Trans.* **2015**, *44*, 7835–7843.
[41] M. Jalalah, M. Faisal, H. Bouzid, J.-G. Park, S. A. Al-Sayari, A. A. Ismail, *J. Ind. Eng. Chem.* **2015**, *30*, 183–189.
[42] H.-Y. Jiang, P. Li, G. liu, J. Ye, J. Lin, *J. Mater. Chem. A* **2015**, *3*, 5119–5125.
[43] Y. Yan, Z. Zhou, Y. Cheng, L. Qiu, C. Gao, J. Zhou, *J. Alloys Compd.* **2014**, *605*, 102–108.
[44] J. Wang, X. Yang, K. Zhao, P. Xu, L. Zong, R. Yu, D. Wang, J. Deng, J. Chen, X. Xing, *J. Mater. Chem. A* **2013**, *1*, 9069–9074.
[45] J. Liqiang, Q. Yichun, W. Baiqi, L. Shudan, L. Baojiang, Y. Libin, F. Wei, F. Honggang, S. Jiazhong, *Sol. Energy Mater. Sol. Cells* **2006**, *90*, 1773–1787.
[46] X. Du, Y. Liu, X. Wang, J. Feng, C. Ren, *J. Aust. Ceram. Soc.* **2019**, *55*, 71–76.
[47] Q. Wang, C. Chen, D. Zhao, W. Ma, J. Zhao, *Langmuir* **2008**, *24*, 7338–7345.
[48] H. Park, W. Choi, *J. Phys. Chem. B* **2005**, *109*, 11667–11674.
[49] P. Pichat, *Photocatalysis and Water Purification*, Wiley-VCH Verlag GmbH & Co. KGaA, Weinheim **2013**.
[50] S. Iyyapushpam, S. T. Nishanthi, D. P. Padiyan, *J. Phys. Chem. Solids* **2015**, *81*, 74–78.
[51] Y. Lu, Y. Zhao, J. Zhao, Y. Song, Z. Huang, F. Gao, N. Li, Y. Li, *Cryst. Growth Des.* **2015**, *15*, 1031–1042.
[52] J. Eberl, H. Kisch, *Z. Naturforsch. B* **2010**, *65*, 399–404.
[53] J. L. Ortiz-Quiñonez, C. Vega-Verduga, D. Díaz, I. Zumeta-Dubé, *Cryst. Growth Des.* **2018**, *18*, 4334–4346.
[54] Z. Ni, Y. Sun, Y. Zhang, F. Dong, *Appl. Surf. Sci.* **2016**, *365*, 314–335.
[55] C. Greaves, S. K. Blower, *Mater. Res. Bull.* **1988**, *23*, 1001–1008.
[56] R. W. Engle, US Patent 20,120,241,478 **2012**.
[57] R. C. Dykhuizen, M. F. Smith, *J. Therm. Spray Technol.* **1998**, *7*, 205–212.
[58] J. Tauc, R. Grigorovici, A. Vancu, *Phys. Status Solidi B* **1966**, *15*, 627–637.